J|A|C|S ARTICLES

Published on Web 03/06/2009

Analysis of the UV/Vis and CD Spectral Line Shapes of Carotenoid Assemblies: Spectral Signatures of Chiral *H*-Aggregates

Frank C. Spano

Department of Chemistry, Temple University, Philadelphia, Pennsylvania 19122

Received August 29, 2008; E-mail: spano@temple.edu

Abstract: Using vibronic exciton theory we evaluate the absorption and CD spectra of lutein and lutein diacetate aggregates, which have previously been described as card-packed *H*-aggregates and head-to-tail *J*-aggregates, respectively. The dramatically different spectral line shapes for *both* aggregates are shown to arise from strongly and weakly coupled *H*-aggregates consisting of helical arrays of chromophores. For lutein, the aggregates consist of tightly packed stacks of individual carotenoid molecules, while lutein diacetate aggregates resemble nematic liquid crystals. For both aggregates the agreement between experiment and theory is excellent. Analytical expressions for the absorption and CD spectra are presented, highlighting the spectral signatures of weakly coupled *H* (and *J*)-aggregation arising from distortions in the single-molecule Franck−Condon progression.

I. Introduction

Carotenoids play many essential roles in biology. They are involved in light harvesting[1,2] and photoprotection[3,4] in photosynthesis and serve as the primary component of many plant pigments.[5] They have also been extensively studied as antioxidants,[6] with many potential health benefits in humans.[7−9]

Many carotenoids are known to aggregate in aqueous mixtures due to strong hydrophobic forces.[10−19] Chiral carotenoids form helical aggregates in which the polyene cores are believed to π-stack while maintaining a relative overlay angle ϕ between neighboring molecules. Intermolecular interactions within carotenoid assemblies result in significant spectral shifts, important, for example, in defining the color of flower petals.[5] Such aggregates also serve as excellent model systems for studying intermolecular interactions in conjugated molecular systems with more complex morphologies, such as polymer films. In poly(3-hexylthiophene) (P3HT) films used in solar cells[20,21] and transistors,[22,23] intra- and intersegment π-stacking and exciton−vibrational coupling very similar to that displayed in carotenoid aggregates play a major role in determining the photophysics.[24−26] The chirality of the carotenoid aggregates has an added bonus of admitting investigations using circularly polarized light, allowing for more rigorous testing of recent theoretical approaches.[27−31]

The catalog of absorption and CD spectra for carotenoid aggregates is quite rich,[11−14,16−19] but two extremes are clearly identified.[12] In one, the absorption spectrum is dominated by a

(1) Vaswani, H. M.; Holt, N. E.; Fleming, G. R. *Pure Appl. Chem.* **2005**, *77*, 925.
(2) Polivka, T.; Sundstrom, V. *Chem. Rev.* **2004**, *104*, 2021.
(3) Holt, N. E.; Zigmantas, D.; Valkunas, L.; Li, X. P.; Niyogi, K. K.; Fleming, G. R. *Science* **2005**, *307*, 433.
(4) Avenson, T. J.; Ahn, T. K.; Zigmantas, D.; Niyogi, K. K.; Li, Z.; Ballottari, M.; Bassi, R.; Fleming, G. R. *J. Biol. Chem.* **2008**, *283*, 3550.
(5) Zsila, F.; Deli, J.; Simonyi, M. *Planta* **2001**, *213*, 937.
(6) Bohm, F.; Edge, R.; Land, E. J.; McGarvey, D. J.; Truscott, T. G. *J. Am. Chem. Soc.* **1997**, *119*, 621.
(7) Calvo, M. M. *Crit. Rev. Food Sci. Nutr.* **2005**, *45*, 671.
(8) Perera, C. O.; Yen, G. M. *Int. J. Food Prop.* **2007**, *10*, 201.
(9) Shixian, Q.; Da, Y.; Kakuda, Y.; Shi, J.; Mittal, G.; Yeung, D.; Jiang, Y. *Food Rev. Int.* **2005**, *21*, 295.
(10) Horn, D.; Rieger, J. *Angew. Chem., Int. Ed.* **2001**, *40*, 4331.
(11) Ruban, A. V.; Horton, P.; Young, A. J. J. *Photochem. Photobiol. B* **1993**, *21*, 229.
(12) Simonyi, M.; Bikadi, Z.; Zsila, F.; Deli, J. *Chirality* **2003**, *15*, 680.
(13) Zsila, F.; Bikadi, Z.; Keresztes, Z.; Deli, J.; Simonyi, M. *J. Phys. Chem. B* **2001**, *105*, 9413.
(14) Zsila, F.; Bikadi, Z.; Deli, J.; Simonyi, M. *Tetrahedron Lett.* **2001**, *42*, 2561.
(15) Bikadi, Z.; Zsila, F.; Deli, J.; Mady, G.; Simonyi, M. *Enantiomer* **2002**, *7*, 67.
(16) Wang, L.; Du, Z.; Li, R.; Wu, D. *Dyes Pigments* **2005**, *65*, 15.
(17) Kopsel, C.; Moltgen, H.; Schuch, H.; Auweter, H.; Kleinermanns, K.; Martin, H. D.; Bettermann, H. J. *Mol. Struct.* **2005**, *750*, 109.
(18) Auweter, H.; Haberkorn, H.; Heckmann, W.; Horn, D.; Luddecke, E.; Rieger, J.; Weiss, H. *Angew. Chem., Int. Ed.* **1999**, *38*, 2188.
(19) Billsten, H. H.; Sundstrom, V.; Polivka, T. *J. Phys. Chem. A* **2005**, *109*, 1521.
(20) Brabec, C. J.; Dyakonov, V.; Parisi, J.; Sariciftci, N. S. *Organic photovoltaics: concepts and realization*; Springer: Heidelberg, 2003.
(21) Erb, T.; Zhokhavets, U.; Gobsch, G.; Raleva, S.; Stuhn, B.; Schilinsky, P.; Waldauf, C.; Brabec, C. J. *Adv. Funct. Mater.* **2005**, *15*, 1193.
(22) Yang, Y.; Heeger, A. J. *Nature* **1994**, *372*, 344.
(23) Bao, Z.; Dodabalapui, A.; Lovinger, A. J. *Appl. Phys. Lett.* **1996**, *69*, 4108.
(24) Clark, J.; Silva, C.; Friend, R. H.; Spano, F. C. *Phys. Rev. Lett.* **2007**, *98*, 206406.
(25) Brown, P. J.; Thomas, S. D.; Kohler, A.; Wilson, J. S.; Kim, J.-S.; Ramsdale, C. M.; Sirringhaus, H.; Friend, R. H. *Phys. Rev. B* **2003**, *67*, 064203.
(26) Chang, J. F.; Clark, J.; Zhao, N.; Sirringhaus, H.; Breiby, D. W.; Andreasen, J. W.; Nielsen, M. M.; Giles, M.; Heeney, M.; McCulloch, I. *Phys. Rev. B* **2006**, 74.
(27) Eisfeld, A.; Kniprath, R.; Briggs, J. S. *J. Chem. Phys.* **2007**, *126*, 104904.
(28) Didraga, C.; Knoester, J. *J. Chem. Phys.* **2004**, *121*, 10687.
(29) Didraga, C.; Klugkist, J. A.; Knoester, J. *J. Phys. Chem. B* **2002**, *106*, 11474.
(30) Spano, F. C.; Meskers, S. C. J.; Hennebicq, E.; Beljonne, D. *J. Am. Chem. Soc.* **2007**, *129*, 7044; **2007**, *129*, 16278 (erratum).

single intense peak, blue-shifted by approximately 5000−6000 cm^{-1} relative to the solvated molecule (monomer) spectrum. The corresponding CD spectrum consists of a classic bisignate couplet which passes through zero near the absorption peak. This aggregate has been referred to as a tightly packed or "card-packed" *H*-aggregate. In the other extreme, the aggregate spectrum is slightly red-shifted (<1000 cm^{-1}) but displays complex vibronic structure with peak intensities that no longer conform to the Poissonian Franck−Condon progression found in the monomer absorption spectrum. Due to aggregation, the 0−0 peak is substantially suppressed relative to the 0−1 peak. Moreover, the vibronic satellites are not displaced by regular multiples of the vibrational frequency (ω_0) from the 0−0 origin. In particular, the 0−0/0−1 spectral separation is significantly larger than ω_0.[12,13,19] The associated CD spectrum also displays complex vibronic structure and is not proportional to the derivative of the absorption spectra. This aggregate has been universally described as a "head-to-tail" *J*-aggregate based solely on the overall red-shift of the absorption spectrum compared to the monomer spectrum.

In much of the literature on carotenoid aggregates, the assignment of *J*- vs *H*-aggregation is made solely on the basis of the sign of the aggregation-induced (absorption) spectral shifts. However, such shifts have two origins: the resonant excitonic shift, whose sign depends on the sign of the intermolecular interactions, and the nonresonant dispersive shift, sometimes referred to as a gas-to-crystal shift, which is usually negative. The spectral shift definition therefore leads to some ambiguity in the case of weakly coupled *H*-aggregates, where the blue-shift from excitonic interactions can be much smaller than the red-shift due to nonresonant interactions. In addition, the entire *J* vs *H* assignment is unambiguous for only the simplest packing geometries (for example, one-dimensional arrays). For more complex structures, such as the layered helices considered in this work, a given molecule can simultaneously experience substantial negative (i.e., head- to-tail) and positive (i.e., side-by-side) interactions, resulting in an unusual "hybrid" optical response where the absorption and CD line shapes reflect *H*-aggregation but with an overall excitonic red-shift.

In this work we investigate theoretically absorption and circular dichroism in lutein and lutein diacetate aggregates. Zsila and co-workers[13] showed that, by simply replacing the two hydroxyl hydrogen atoms in a lutein molecule by $COCH_3$ groups, the aforementioned tightly packed *H*-aggregates are converted to loosely packed "*J*-aggregates". In treating the exciton−vibrational coupling involving the progression forming intramolecular vibration, we utilize a basis set consisting of vibronic excitons and vibronic/vibrational pair excitons,[30] pioneered by Philpott[32] and used successfully by us to account for the photophysics of a variety of materials, including molecular aggregates and crystals,[33−36] hydrogen-bonded self-assemblies,[30,37] and polymer films.[38,39] In what follows we evaluate the absorption and CD spectra for model lutein and lutein diacetate aggregates numerically and also analytically in the weak coupling regime, using the single-particle approximation. We carefully delineate the spectral signatures of weakly coupled *H*- and *J*-aggregates, showing that the measured spectra for lutein diacetate aggregates are better characterized as weakly coupled *H*-aggregates resembling nematic liquid crystals and not *J*-aggregates, as had been previously assumed.

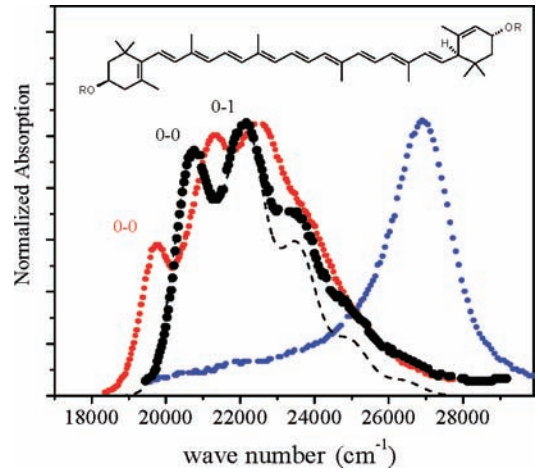

Figure 1. Absorption spectrum of lutein in acetone (black), lutein in an aqueous acetone mixture (blue), and lutein diacetate in aqueous acetone (red), taken from ref 13. The spectrum for lutein diacetate in acetone (not shown) is essentially unchanged from the lutein/acetone spectrum, differing only in a small blue-shift of less than 1 nm. Also shown (dashed curve) is a fit to the lutein acetone spectrum using the vibronic progression in eq 1 with $\omega_0 = 1400$ cm^{-1}, an HR factor of $\lambda^2 = 1.1$ and with $\omega_{0-0} + D = 20\,800$ cm^{-1}. The discrepancy at higher energies is most likely due to enhanced scattering in the measured spectrum. Inset shows molecular structure of lutein (R = H) and lutein diacetate (R = $COCH_3$).

II. Absorption in Lutein and Lutein Diacetate Aggregates

We begin by reviewing the absorption and CD spectra of lutein and lutein diacetate in acetone and in aqueous acetone mixtures. The spectra from ref 13 are reproduced in Figure 1. The black curve shows lutein dissolved in acetone. Since acetone is a good solvent, the spectrum reflects solvated single molecules. The vibronic progression is due to the coupling of the optically allowed $S_0 \rightarrow S_2$ transition to a symmetric vinyl stretching mode with frequency $\omega_0 \approx 0.173$ $eV/\hbar$ (1400 cm^{-1}). S_2 correlates to the 1^1B_u state in polyenes, which lies energetically above the dark $2^1A_g(S_1)$ state.[2,19] Although not shown, the spectrum for lutein diacetate in acetone is essentially identical except for a small (<1 nm) blue-shift.[13]

Aggregation is initiated upon the addition of water, leading to a dramatic spectral blue-shift with the complete loss of vibronic structure in the case of lutein, and to a red-shifted distorted vibronic progression in the case of lutein diacetate. On the basis of the sign of the aggregation-induced spectral shift, the lutein aggregates have been described as "card-packed" *H*-aggregates, while the lutein diacetate aggregates have been universally described as "head-to-tail" *J*-aggregates. In what follows, we show that the spectral line shapes for both aggregates are characteristic of *H*-aggregates, differing only in the magnitude of excitonic bandwidth. The red-shift of the lutein diacetate spectrum is not conclusive evidence for *J*-aggregation (i.e., predominant head-to-tail coupling) since the shift is also due to nonresonant ("gas-to-crystal") coupling.

(31) Beljonne, D.; Hennebicq, E.; Daniel, C.; Herz, L. M.; Silva, C.; Scholes, G. D.; Hoeben, F. J. M.; Jonkheijm, P.; Schenning, A. P. H. J.; Meskers, S. C. J.; Phillips, R. T.; Friend, R. H.; Meijer, E. W. *J. Phys. Chem B* **2005**, *109*, 10594.
(32) Philpott, M. R. *J. Chem. Phys.* **1971**, *55*, 2039.
(33) Spano, F. C. *J. Chem. Phys.* **2002**, *116*, 5877.
(34) Spano, F. C. *J. Chem. Phys.* **2003**, *118*, 981.
(35) Spano, F. C. *J. Chem. Phys.* **2004**, *120*, 7643.
(36) Spano, F. C. *Annu. Rev. Phys. Chem.* **2006**, *57*, 217.
(37) Spano, F. C.; Meskers, S. C. J.; Hennebicq, E.; Beljonne, D. *J. Chem. Phys.* **2008**, *129*, 024704.
(38) Spano, F. C. *J. Chem. Phys.* **2005**, *122*, 234701.
(39) Spano, F. C. *Chem. Phys.* **2006**, *325*, 22.

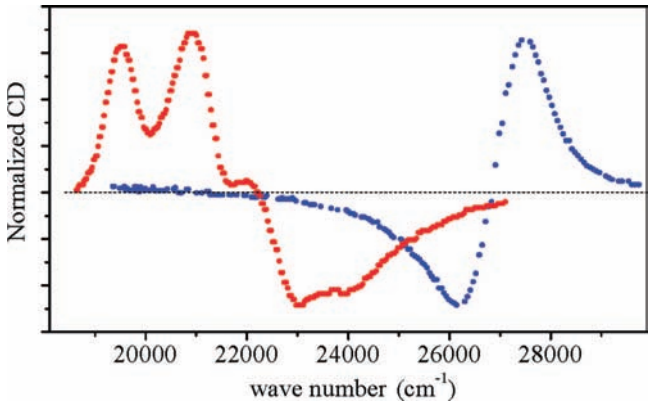

Figure 2. CD spectrum of lutein diacetate in aqueous acetone (red) and lutein in aqueous acetone (blue) from ref 13. The spectrum for lutein or lutein diacetate in acetone has negligible CD activity in the spectral window shown.

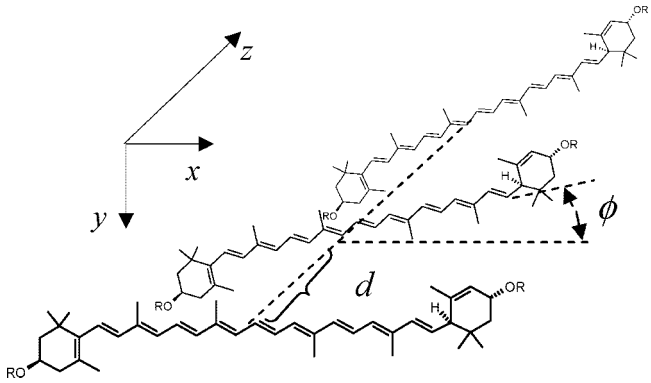

Figure 3. Model *H*-aggregate defined by the overlay or pitch angle, ϕ, and the nearest-neighbor separation, *d*. Positive (negative) ϕ defines a left (right)-handed helix.

An additional spectroscopic clue for the aggregate structure lies in the strong aggregation-induced CD response in the spectral window of Figure 1, as reproduced from ref 13 in Figure 2. Although not shown, there is essentially no CD activity for lutein or lutein diacetate dissolved in acetone in the same spectral range; hence, the chiral centers of the individual molecules do not significantly contribute to the CD activity between 325 and 550 nm. Lutein aggregates display a classic bisignate Cotton effect attributed to exciton coupling, while the lutein diacetate spectrum shows an overall bisignate effect, but of opposite sign to the lutein aggregates and with complex vibronic structure.

III. Model Aggregate and Hamiltonian

To theoretically account for the spectral signatures of carotenoid aggregates as outlined in the previous section, we employ the aggregate geometry depicted in Figure 3 and introduced in ref 13 to describe the tightly "card-packed" lutein *H*-aggregates. The handedness of the π-stacked helices is directed by the chiral centers of the individual molecules. The lutein enantiomer investigated here has three chiral centers (see Figure 1), as indicated in the formula, (3*R*,3′*R*,6′*R*)-β,ϵ-carotene-3,3′-diol (R = H).[13] Each helical aggregate in Figure 3 consists of *N* coupled chromophores.

The aggregate geometry in Figure 3 is described by the nearest-neighbor separation, *d*, and the "overlay" or pitch angle, ϕ. The model is identical to that used in MOPV4 assemblies to successfully describe polarized absorption and emission.[30,31,37]

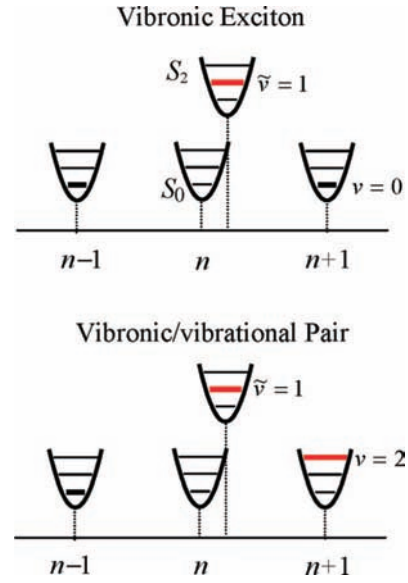

Figure 4. Examples of the fundamental excitations in ordered organic assemblies. The vibronic (single-particle) excitation is $|n, \tilde{v} = 1\rangle$, while the vibronic/vibrational pair (two-particle state) is $|n, \tilde{v} = 1; n + 1, v = 2\rangle$.

In contrast to former work on carotenoid aggregates,[12,13] we employ the aggregate model in Figure 3 to also account for lutein diacetate aggregates. Previous works[12,13] utilized "head-to-tail" geometries to describe carotenoids aggregates showing spectral signatures similar to the red curves in Figures 1 and 2.

In developing a semiempirical Hamiltonian for the aggregates in Figure 3, we utilize the spectral information of individual lutein or lutein diacetate molecules shown in Figure 1. The vibronic progression in the molecular absorption spectrum derives from harmonic ground- and excited-state nuclear potentials, with the potential corresponding to the excited state S_2 shifted relative to that of the ground state S_0 as depicted in Figure 4 (refer to the *n*th molecule in the top panel). In this case the absorption spectrum takes the form of a vibronic progression with peak intensities given by Franck−Condon (FC) factors:

$$A(\omega) = \sum_{v=0,1,2,\ldots} \frac{\lambda^{2v} e^{-\lambda^2}}{v!} \Gamma(\omega - \omega_{0-0} - D_{sol} - v\omega_0) \qquad (1)$$

where λ^2 is the Huang−Rhys (HR) factor, ω_{0-0} is the gas-phase 0−0 transition frequency, D_{sol} is the solvent shift in acetone, and ω_0 is the vibrational frequency. Figure 1 shows a successful fit using eq 1 with the Gaussian line shape,

$$\Gamma(\omega) = \exp(-\omega^2/\sigma^2). \qquad (2)$$

From the fit we obtain $\sigma = 728$ cm^{-1}, $\lambda^2 = 1.1$, $\omega_{0-0} + D_{sol} = 20\,800$ cm^{-1} and $\omega_0 = 1400$ cm^{-1}. (In reporting frequencies in units of wave numbers we have tacitly assumed $2\pi c = 1$.)

In developing the aggregate Hamiltonian, let us first neglect the excitonic coupling. In this case the lowest energy eigenstates consist of the localized vibronic and vibronic/vibrational pair states depicted in Figure 4. Such states are generally classified as multi-particle states beginning with the single-particle excitation, $|n, \tilde{v}\rangle$, consisting of a vibronically excited chromophore at site *n* with $\tilde{v}$ excited-state quanta in the (shifted) excited state (S_2) nuclear potential and with all other molecules electronically and vibrationally unexcited. The corresponding transition energy relative to the electronic ground state with no vibrational energy is

$$e_{n,\tilde{v}} = \omega_{0-0} + D_{\mathrm{agg}} + \tilde{v}\omega_0 \tag{3}$$

where D_{agg} is the gas-to-crystal shift due to nonresonant interactions, and we have taken $\hbar = 1$.

A vibronic/vibrational *pair* excitation, denoted $|n, \tilde{v}; n', v'\rangle$, is a two-particle state. In addition to a vibronic excitation at n, this state includes a *vibrational* excitation at n', with v' (≥ 1) quanta in the ground-state potential, as demonstrated schematically in Figure 4. The energy of the vibronic/vibrational pair state is given by

$$e_{n,\tilde{v};n'v'} = \omega_{0-0} + D_{\mathrm{agg}} + (\tilde{v} + v')\omega_0. \tag{4}$$

One can also identify three-particle and higher states; however, truncating at the two-particle level is highly accurate in the weak to intermediate excitonic coupling regime appropriate for carotenoid aggregates, where the vibrational energy, ω_0, the vibronic relaxation energy, $\lambda^2\omega_0$, and the (free) exciton bandwidth, W, are all comparable in magnitude.

When excitonic coupling is activated, the local states depicted in Figure 4 are no longer eigenstates. The complete Hamiltonian can be written as

$$H = H_0 + H_{\mathrm{ex}} \tag{5a}$$

with

$$H_{\mathrm{ex}} \equiv \sum_{\substack{m,\,n \\ (m\neq n)}} J_{mn}\{|m\rangle\langle n| + |n\rangle\langle m|\}. \tag{5b}$$

H_0 is diagonal in the one- and two-particle basis set with matrix elements given by eqs 3 and 4. The exciton coupling matrix, H_{ex}, accounts for the resonant exciton coupling between the mth and nth molecules, dictated by J_{mn}. Open boundary conditions are taken throughout unless specifically stated otherwise. H_{ex} is expressed in a basis of pure electronic excited states: the state $|n\rangle$ represents chromophore n excited electronically (S_2), while all remaining chromophores are in their electronic ground states (S_0). H_{ex} intermixes the single- and two-particle states from Figure 4. The mixing is modulated by λ^2. For example, intermixing within the vibronic (one-particle) states is dictated by the matrix elements,

$$\langle m,\tilde{v}|\, H_{\mathrm{ex}}\, |n,\tilde{v}'\rangle = J_{mn} f_{\tilde{v},0} f_{\tilde{v}',0}$$

where the overlap between the harmonic oscillator eigenfunction with $\tilde{v}$ quanta in the shifted excited S_2 potential and that with v quanta in the ground S_0 potential is given by $f_{\tilde{v},v} \equiv \langle\tilde{v}|v\rangle$. For harmonic wells as assumed here, $f_{\tilde{v},0} \equiv \lambda^{\tilde{v}} \exp(-\lambda^2/2)/\sqrt{(\tilde{v}!)}$.

The matrix element connecting the single- and two-particle states in Figure 4 is given by

$$\langle m,\tilde{v}|\, H_{\mathrm{ex}}\, |n,\tilde{v}';n',v'\rangle = J_{nn'} f_{\tilde{v},v'} f_{\tilde{v}',0}\, \delta_{mn'}.$$

The remaining matrix elements representing intermixing with the two-particle manifold are straightforward and are not shown. Finally, we point out that H in eq 5a is identical to the Holstein Hamiltonian reported in earlier works,[36,38,39] when truncating the basis at the two-particle level.

The excitonic couplings J_{mn} between chromophores at m and n are computed using the "supermolecular" dimer approach of ref 40, using an unscreened Coulombic potential for (transition) charges on separate molecules. Details are included in the Supporting Information. Our interactions agree very favorably with the polyene interactions calculated by Beljonne et al.[41] and reduce to the simple point-dipole/point-dipole form when the intermolecular separation greatly exceeds the conjugation length. Figure 5 shows $J_{n,n+s}$ as a function of separation s for the model aggregate shown in Figure 5, with an overlay angle of 20°. The sign change around $s = 5$ occurs when the relative angle between the transition dipole moments ($s\phi$) surpasses 90°, a result consistent with point-dipole/point-dipole coupling.

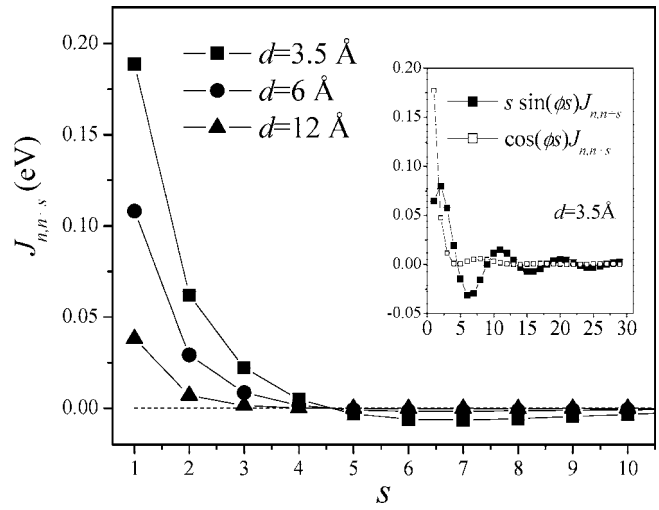

Figure 5. Excitonic coupling $J_{n,n+s}$ as a function of intermolecular distance, sd, for chiral aggregates with overlay angle $|\phi| = 20°$, and selected values of nearest-neighbor separation, d. Inset shows the cosine-modulated interactions responsible for the exciton shift and the much longer range $s\sin(\phi s)$-modulated interactions responsible for the strength of the CD signal (for $d = 3.5$ Å). All interactions are symmetric in s. (Only $s > 0$ interactions are shown.)

Within the two-particle approximation, the αth eigenstate of H can be expanded in one- and two-particle states:

$$|\psi^{(\alpha)}\rangle = \sum_{n,\tilde{v}} c^{(\alpha)}_{n,\tilde{v}}\, |n,\tilde{v}\rangle + \sum_{n,\tilde{v}} \sum_{n',v'} c^{(\alpha)}_{n,\tilde{v};n'v'}\, |n,\tilde{v};n',v'\rangle. \tag{6}$$

In disorder-free aggregates such states are delocalized over the entire π-stack. They can be described as neutral (excitonic) polarons since the electronic excitation is dressed by intramolecular vibrations. States in eq 6 that correlate to single-particle states in the limit of vanishing excitonic coupling form vibronic exciton bands, as discussed in greater detail in section V. Such vibronic states dominate the absorption, as pure two-particle states are dark states. However, as we will show, the two-particle component in (6) increases with the exciton bandwidth, leading to significant changes to the absorption and CD line shapes.

IV. Absorption in Helical Stacks

In what follows we evaluate the unpolarized absorption spectrum, $A(\omega)$, and the circular dichroism spectrum, $\mathrm{CD}(\omega)$, for the model aggregates of Figure 3 using the expressions

$$A(\omega) = \sum_{\alpha} d_\alpha \Gamma(\omega - \omega_\alpha) \tag{7a}$$

and

$$\mathrm{CD}(\omega) = \sum_{\alpha} R_\alpha \Gamma(\omega - \omega_\alpha) \tag{7b}$$

respectively, where $\Gamma(\omega - \omega_\alpha)$ is a symmetric line shape function centered about the energy, ω_α, of the αth eigenstate. We continue to use the Gaussian form of $\Gamma(\omega - \omega_\alpha)$ in eq 2, with the line width σ determined from the monomer spectrum. The associated absorption and rotational line strengths in eqs 7a and 7b are given by

(40) Siddiqui, S.; Spano, F. C. *Chem. Phys. Lett.* **1999**, *308*, 99.
(41) Beljonne, D.; Cornil, J.; Silbey, R.; Millie, P.; Bredas, J. L. *J. Chem. Phys.* **2000**, *112*, 4749.

$$d_\alpha = \frac{1}{\mu^2}\left|\sum_n \langle \psi^{(\alpha)}| \hat{\boldsymbol{\mu}}_n |G\rangle\right|^2 \tag{8a}$$

and[42]

$$R_\alpha = \frac{k_\lambda}{\mu^2}\sum_{n,n'} \langle \psi^{(\alpha)}| \hat{\boldsymbol{\mu}}_n |G\rangle \times \langle G|\hat{\boldsymbol{\mu}}_{n'}|\psi^{(\alpha)}\rangle \cdot (\boldsymbol{r}_n - \boldsymbol{r}_{n'}) \tag{8b}$$

where $|G\rangle$ is the ground state of the aggregate in which all molecules are electronically and vibrationally unexcited. In addition, $k_\lambda \equiv \omega_{0-0}/c$, and $\boldsymbol{\mu}_n$ is the molecular transition dipole. The latter is directed mainly (although not entirely) along the long molecular axis.[43] Based on the right-hand coordinate system in Figure 3, the dipole moment operator for the nth molecule is

$$\hat{\boldsymbol{\mu}}_n = \mu\{|n\rangle\langle g| + |g\rangle\langle n|\}[\cos(\phi n)\boldsymbol{i} - \sin(\phi n)\boldsymbol{j}] \tag{9}$$

corresponding to a left-handed (right-handed) helix for $\phi > 0$ ($\phi < 0$). Here $|g\rangle$ is the pure electronic ground state of the aggregate (no vibrational coordinates), and the local electronic excited state $|n\rangle$ was defined after eq 5b.

Inserting the wave function (6) into eqs 8a and 8b gives the line strengths in terms of the multiparticle coefficients,

$$d_\alpha = \sum_{n,n'}\sum_{\tilde{v},\tilde{v}'} c^{(\alpha)}_{n,\tilde{v}}\, c^{(\alpha)}_{n',\tilde{v}'} f_{\tilde{v}0} f_{\tilde{v}'0} \cos[\phi(n-n')] \tag{10a}$$

$$R_\alpha = k_\lambda d \sum_{n,n'}\sum_{\tilde{v},\tilde{v}'} c^{(\alpha)}_{n,\tilde{v}}\, c^{(\alpha)}_{n',\tilde{v}'} f_{\tilde{v}0} f_{\tilde{v}'0}(n'-n)\sin[\phi(n'-n)]. \tag{10b}$$

Equations 10a and 10b show that only one-particle coefficients directly contribute to the line strengths. Two-particle coefficients contribute indirectly through wave function renormalization. As shown in refs 33−35, the two-particle coefficients contribute directly to the *emission* line strengths, enabling the polaron radius to be evaluated from the circularly polarized emission.[30]

Using the molecular parameters gleaned from the spectrum in Figure 1 for the molecularly dissolved species ($\omega_0 = 1400$ cm^{-1}, $\lambda^2 = 1.1$, $\sigma = 728$ cm^{-1}) along with the couplings J_{mn} evaluated for the d values shown in Figure 5 with $\phi = -20°$, we represented the Hamiltonian, H, in eq 5a in the one- and two-particle basis set depicted in Figure 4. We also took $\omega_{0-0} + D_{agg} = 20\,800$ cm^{-1} ($D_{agg} = D_{sol}$) so that, at this level, all spectral shifts are attributable to resonant excitonic interactions. (We relax this restriction when comparing to experiment in section VI). After obtaining the one- and two-particle coefficients of all eigenstates numerically, we computed the absorption and CD spectra using eqs 7a and 8a. We also calculated the spectra using only the one-particle states. Results for aggregates containing $N = 30$ chromophores are shown in Figure 6.

Figure 6a shows how the absorption spectrum evolves from the weak/intermediate excitonic coupling regime ($W < \omega_0\lambda^2$), corresponding to $d = 12$ Å and $W = 1260$ cm^{-1}, to the strong excitonic coupling regime ($W \gg \omega_0\lambda^2$) corresponding to the closest spacing, $d = 3.5$ Å, and $W = 6520$ cm^{-1}. Here, W is the free exciton bandwidth evaluated directly from H_{ex} in eq 5b. The figure shows how the vibronic structure is lost and the spectral centroid shifts to the blue as W increases, in a manner similar to that shown by Eisfeld and Briggs[44] using the CES approximation. Note that the two-particle states become increasingly important as the exciton bandwidth increases. We also evaluated the spectra using three-particle states, which showed essentially no change from the two-particle spectra (not shown).

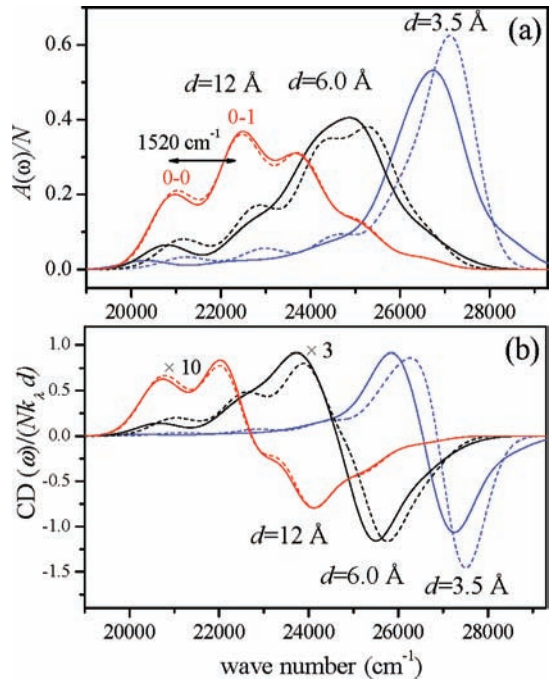

Figure 6. Calculated absorption (a) and CD (b) spectra for right-handed carotenoid aggregates with overlay angle $\phi = -20°$ and for several values of nearest-neighbor distance d. Aggregates contain $N = 30$ chromophores,which is large enough to ensure convergence in the spectral line shapes. Dashed curves were evaluated using only single-particle states. Intermolecular interactions were taken from Figure 5. In all cases, $\omega_0 = 1400$ cm^{-1}, $\lambda^2 = 1.1$, and $\omega_{0-0} + D_{agg} = 20\,800$ cm^{-1} (i.e., $D_{agg} = D_{sol}$).

The spectrum for the strongest coupling is dominated by a single intense peak, blue-shifted by 5900 cm^{-1} from the 0−0 peak in the monomer spectrum (~20 800 cm^{-1}, see Figure 1). In this case the coupling is so strong that the exciton coherently jumps to a neighbor before any significant nuclear relaxation can occur, thereby accounting for the lack of vibronic structure. Under these conditions the blue-shift is approximately given by the unrelaxed free exciton value,

$$\Delta_{ex} = J_\phi + \lambda^2\omega_0 \tag{11}$$

where

$$J_\phi \equiv 2\sum_{s>0} J_{n,n+s}\cos(\phi s) \tag{12}$$

is the excitonic contribution to the energy of the optically allowed degenerate excitons with wave vectors, $k = \pm\pi\phi/180$, with ϕ expressed in degrees.[27,29] This is consistent with the selection rule for perpendicular transitions in long helical aggregates, $\Delta k = \pm 2\pi/M$, where M is the number of chromophores within a complete helical turn.[27,29] Equations 11 and 12 are rigorously correct when N is sufficiently large that the absorption and CD spectra (normalized to N) no longer change with increasing N. For the aggregates in Figure 6, convergence is ensured by approximately $N = 30$.

The cosine-modulated interactions in J_ϕ for the tightly packed aggregate in Figure 6 are shown in the inset of Figure 5, from which we obtain $J_\phi = 4270$ cm^{-1}. According to eq 11, Δ_{ex} is therefore 5810 cm^{-1}, in close agreement with the value of 5900

(42) *Circular Dichroism Principles and Applications*; Nakanishi, K., Berova, N., Woody, R. W., Eds.; Wiley-VCH: New York, 2000.
(43) The transition dipole moment is actually within the plane of the molecule but slightly tilted away from the long axis by about 10°, as shown by our semiempirical calculations.
(44) Eisfeld, A.; Briggs, J. S. *Chem. Phys.* **2006**, *324*, 376.

cm^{-1} obtained from Figure 6a. Comparison of the spectrum in Figure 6a with the absorption spectrum for unrelaxed free excitons,

$$A(\omega)/N = \Gamma(\omega - \omega_{0-0} - D_{agg} - J_\phi - \lambda^2\omega_0) \qquad (13)$$

shows that the (unit) peak intensity of the latter is roughly twice as large as the peak intensity in Figure 6a, due to a significant amount of oscillator strength which remains in the long tail on the red side of the main peak. We have verified that, with increasing exciton bandwidth, the oscillator strength in the red tail diminishes while that in the main peak increases.[33] When $W \gg \lambda^2\omega_0$, the absorption spectrum calculated using the full one- and two-particle basis set approaches that in eq 13.

The corresponding CD spectrum for the tightly packed aggregate in Figure 6b displays the classic bisignate Cotton effect, crossing zero at the peak of the absorption line. Appealing once again to the free exciton behavior, the CD spectrum is approximately given by

$$\mathrm{CD}(\omega)/N = 4k_\lambda d \times \left\{\sum_{s>0} J_{m,m+s}\, s\, \sin(\phi s)\right\} \frac{\omega - \omega_{0-0} - D_{agg} - J_\phi - \lambda^2\omega_0}{\sigma^2} \times \Gamma(\omega - \omega_{0-0} - D_{agg} - J_\phi - \lambda^2\omega_0). \qquad (14)$$

We derived eq 14 using a procedure similar to that employed by Harada et al.,[45] in which the Gaussian line function appearing in eq 7b is Taylor-expanded in the small deviations $(J_k - J_\phi)/\sigma$, where J_k is the exciton interaction sum for the kth exciton. The CD spectrum in eq 14 agrees with that derived by Didraga et al.[29] for the special case of radially directed transition dipole moments.

Equation 14 shows that the magnitude of the CD A value, obtained by subtracting the CD minimum from the maximum, is given by

$$|A_{CD}| = 2^{5/2}\, e^{-1/2}\, \frac{k_\lambda d}{\sigma} \sum_{s>0} J_{m,m+s}\, s\, \sin(\phi s). \qquad (15)$$

The value of $|A_{CD}|/k_\lambda d$ in eq 15 is roughly thrice that obtained from the value of ≈ 2 in Figure 6, due to the significant (rotational) line strength residing in the red tail.

The $s\sin(\phi s)$-modulated interaction sum appearing in eqs 14 and 15 is far more sensitive to extended interactions than is the cosine-modulated sum, J_ϕ, responsible for the excitonic shift, as demonstrated in the inset of Figure 5. This arises because $J_{m,m+s}\, s \sin(\phi s)$ scales as $(ds)^{-2}$, while $J_{m,m+s}\cos(\phi s)$ scales as $(ds)^{-3}$, as originally pointed out by Harada et al.,[45] making CD spectroscopy particularly sensitive to long-range interactions.[46−48]

We now turn our attention to the absorption spectrum corresponding to the loosely packed aggregates with $d = 12$ Å in Figure 6a, which is markedly different from the spectrum representing the tightly packed aggregates ($d = 3.5$ Å) just considered. The spectrum retains vibronic structure, with the 0−0 peak weakly blue-shifted by only 170 cm^{-1} relative to the monomer. The peak intensities no longer adhere to the Poisson distribution of eq 1, with the 0−0 peak substantially attenuated, making the 0−0 to 0−1 peak intensity ratio ($\sim$0.54) almost a factor of 2 smaller than is found in the monomer spectrum of Figure 1. In addition, the vibronic peak energies are no longer regularly spaced in multiples of the vibrational energy, ω_0. The largest such distortion is the increased separation between the 0−0 and 0−1 peaks, measuring approximately 1520 cm^{-1}, or $1.085\omega_0$. Distortions in the vibronic peak spacings have been observed in other carotenoid aggregates[12,19] as well as P3HT thin films.[25,39] The associated CD spectrum in Figure 6b also displays complex vibronic structure with an overall bisignate Cotton effect consistent with a right-handed helix. Interestingly, the CD spectrum is not proportional to the first derivative of the absorption spectrum, as is the case in the strong exciton coupling regime. In order to account for the peculiar vibronic behavior observed in both absorption and CD spectra, we turn next to a theory of weakly coupled H-aggregates.

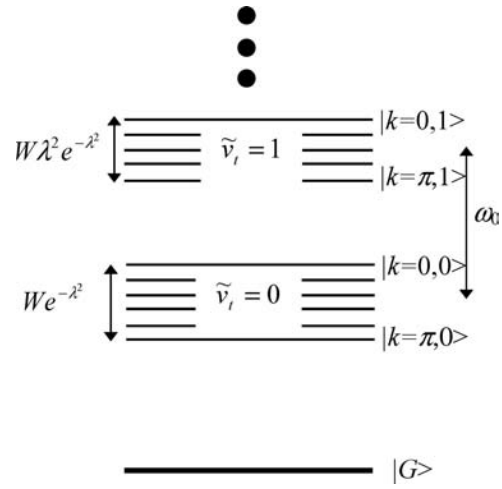

Figure 7. Energy level scheme for weakly coupled H-aggregates showing the lowest two vibronic bands. Wave function labels assume periodic boundary conditions as described in the text. In chiral H-aggregates, oscillator strength is concentrated near the top of each band with $k = \pm\pi\phi/180$. (For the J_{mn} values in Figure 5, the state with $k = 0$ is strictly located on the top of each band for overlay angles ϕ less than approximately 50°.)

V. Weakly Coupled *H*-Aggregates

In this section we investigate the spectral signatures of chiral H-aggregates using perturbation theory. The results are valid under the weak excitonic coupling regime, where the free exciton bandwidth W is much smaller than the vibrational relaxation energy, $\lambda^2\omega_0$. (This is alternately referred to as the strong exciton−phonon coupling regime.) In this regime there exist separate bands of excitons, with each band characterized by the number of vibrational quanta in the shifted (S_2) excited state, as shown in Figure 7. States in the band $\tilde{v}_t$ that are zero-order in the excitonic interaction are the vibronic excitons,

$$|k,\tilde{v}_t\rangle^{(0)} = N^{-1/2}\sum_n c_n^{(k)}|n,\tilde{v}_t\rangle \qquad (16)$$

where the $c_n^{(k)}$ are evaluated by diagonalizing H_{ex} in eq 5b, and k is a quantum number identifying the kth eigenstate. The zero-order states in (16) are correct for $\tilde{v}_t = 0$; however, for higher bands ($\tilde{v}_t \geq 1$), eq 16 neglects the *resonant* coupling between one- and two-particle states (Fermi resonances, see ref 39), for example, between $|n, \tilde{v} = 1\rangle$ and $|n, \tilde{v} = 0; n', v = 1\rangle$ in the $\tilde{v}_t = 1$ band. The neglect is warranted when the associated splittings are much smaller than the peak line widths, an excellent approximation for the carotenoid aggregates studied here.

(45) Harada, N.; Chen, S. L.; Nakanishi, K. *J. Am. Chem. Soc.* **1975**, *97*, 5345.
(46) Matile, S.; Berova, N.; Nakanishi, K.; Fleischhauer, J.; Woody, R. W. *J. Am. Chem. Soc.* **1996**, *118*, 5198.
(47) Lewis, F. D.; Liu, X. Y.; Wu, Y. S.; Zuo, X. B. *J. Am. Chem. Soc.* **2003**, *125*, 12729.
(48) Tsubaki, K.; Takaishi, K.; Tanaka, H.; Miura, M.; Kawabata, T. *Org. Lett.* **2006**, *8*, 2587.

The vibronic excitons in (16) are entirely composed of single-particle states. First-order corrections are dominated by interband mixing between vibronic states with the same k but in different bands (different $\tilde{v}_t$), as well as mixing with two-particle states as described in detail in refs 38 and 39 in the analysis of (achiral) P3HT π-stacks. By generalizing the treatment in refs 38 and 39 to include chiral assemblies (nonzero ϕ) and extended (non-nearest-neighbor) interactions, we arrive at the absorption spectrum for weakly coupled aggregates,

$$A(\omega)/N = \sum_{\tilde{v}_t=0,1,\ldots} f^2_{\tilde{v}_t,0}\left[1-\frac{J_\phi\, e^{-\lambda^2}}{\omega_0}G(\tilde{v}_t;\lambda^2)\right]^2 \Gamma(\omega-\omega_{\pm\phi,\tilde{v}_t}) \tag{17}$$

correct to first order in J_ϕ/ω_0, where J_ϕ, defined in eq 12, is the $k = \pi\phi/180$ Fourier component of the interaction sum, $f^2_{\tilde{v},0} = \lambda^{2\tilde{v}} \exp(-\lambda^2)/\tilde{v}!$ are FC factors, and the function $G(\tilde{v}_t;\lambda^2)$ is given by

$$G(\tilde{v}_t;\lambda^2) \equiv \sum_{\substack{u=0,1,\ldots \\ (u\neq\tilde{v}_t)}} \frac{\lambda^{2u}}{u!\,(u-\tilde{v}_t)}. \tag{18}$$

The derivation of eq 17 assumes long helical π-stacks ($N \gg 1$), with $(N-1)\phi$ taken to be a multiple of 2π without any loss in generality. Equation 17 reduces to our previously derived expression for achiral π-stacks in refs 38 and 39 when $\phi = 0$ and only nearest-neighbor coupling is retained (whence $J_{\phi=0} = W/2$). The details of the derivation will be presented elsewhere.

The form of eq 17 reflects the presence of two (degenerate) optically allowed excitons with wave vectors $k = \pm\pi\phi/180$ in each vibronic band, $\tilde{v}_t$. The $\tilde{v}_t$-dependent line strength consists of the molecular FC factor modulated by an interaction term, $\{1-(J_\phi/\omega_0)\, e^{-\lambda^2}G(\tilde{v}_t;\lambda^2)\}^2$, which is responsible for the vibronic peak distortions. The energy of the optically allowed excitons in the vibronic band $\tilde{v}_t$ is given by $\omega_{\pm\phi,\tilde{v}_t}$. Following the procedure outlined in ref 39 with the extensions made in the present work (extended couplings, nonzero overlay angles), we obtain

$$\omega_{\pm\phi,\tilde{v}_t} = \omega_{0-0} + D_{\mathrm{agg}} + \tilde{v}_t\,\omega_0 + J_\phi f^2_{0,\tilde{v}_t} - \frac{J^2_\phi}{\omega_0} f^2_{0,\tilde{v}_t}\, e^{-\lambda^2}\, G(\tilde{v}_t;\lambda^2) \tag{19}$$

Equation 19 is exact to first order, while the second-order correction is exact only within the single-particle approximation—the complex second-order corrections due to the two-particle states have been neglected.

To test the accuracy of eq 17, we show in Figure 8 absorption spectra for chiral aggregates with $d = 12$ Å and for varying overlay angles, ϕ, calculated fully numerically (see section IV) using the one- and two-particle basis set, as well as perturbatively using eq 17. Each aggregate contains $N = 30$ chromophores, which is enough to ensure convergence; i.e., the spectra are representative of infinitely long helices. Figure 8 shows that the first-order theory does an excellent job in reproducing the exact spectrum as ϕ approaches 90°, or as J_ϕ diminishes due to the decreased intermolecular overlap. Figure 8 also shows the most prominent signature of weak H-aggregation: a decrease in the ratio of the 0−0 to 0−1 line strengths, R_{abs}, with J_ϕ. (There is also a simultaneous increase in the 0−2 intensity relative to the 0−1 intensity.) Based on the perturbation theory result in eq 17, R_{abs} is evaluated as

$$R_{\mathrm{abs}} = \frac{[1-0.496J_\phi/\omega_0]^2}{1.1[1+0.0865J_\phi/\omega_0]^2} \tag{20}$$

where we have used $\lambda^2 = 1.1$ along with $G(0,1.1) = 1.49$ and $G(1,1.1) = -0.260$ from eq 18. Equation 20 explains the demise in R_{abs} with increasing J_ϕ (>0) for H-aggregates with λ^2 near unity. Equation 20 further shows that, in J-aggregates with $J_\phi < 0$, the opposite behavior results: increasing $|J_\phi|$ leads to an *increase* in R_{abs}. This is demonstrated in the inset to Figure 8. Hence, weakly coupled H- and J-aggregates can be easily distinguished on the basis of the effect of aggregation on the 0−0 and 0−1 peak intensities.

Another signature of aggregation in the weak coupling limit is a disruption of the regularity of the vibronic peak energies within the progression. In Figure 6a, the spectral separation between the 0−0 and 0−1 peaks, denoted as Δ_{10}, is significantly larger than ω_0 when $d = 12$ Å: approximately 1520 cm^{-1} compared to $\omega_0 = 1400$ cm^{-1}. Using the perturbation result in eq 19 with $\lambda^2 = 1.1$ gives

$$\Delta_{10}/\omega_0 = 1 + 0.033\frac{J_\phi}{\omega_0} + 0.133\frac{J^2_\phi}{\omega^2_0} \tag{21}$$

which shows both first- and second-order dilations for H-aggregates. (In J-aggregates the first-order term leads to a contraction.) For $\phi = 20°$ ($J_\phi = 0.495\omega_0$), eq 21 predicts an increased spectral separation of 70 cm^{-1}, compared to 120 cm^{-1} obtained numerically. It is clear that the second-order two-particle component, absent in eq 21, contributes significantly to the spectral dilation. It is also instructive to consider the spectral separation between the 0−2 and 0−1 peaks, Δ_{21}. Using eq 19, one can show that Δ_{21} is less than ω_0; i.e., the 0−1 and 0−2 peaks move together upon aggregation. However, whereas Δ_{10} exceeds ω_0 by around 120 cm^{-1}, Δ_{21} is only 35 cm^{-1} below ω_0.

We next evaluate the CD spectrum in the weak coupling limit, working entirely within the single-particle approximation, and utilizing a procedure similar to that employed by Harada et al.[45] After inserting the first-order energies from eq 19 into the CD spectrum in eq 7b, we Taylor-expand the line shape

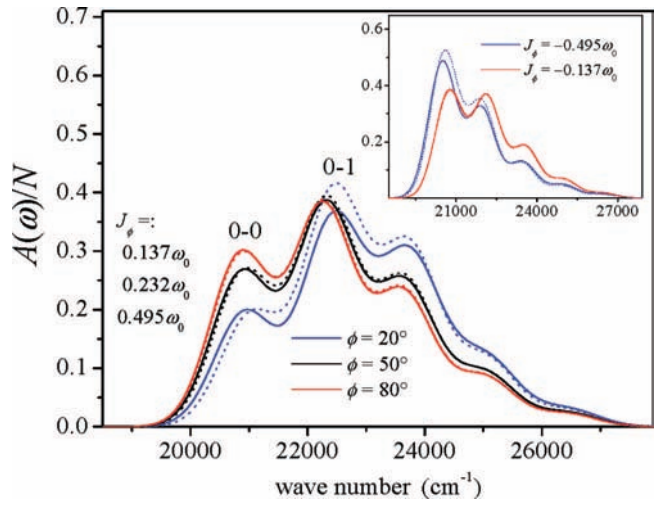

Figure 8. Absorption spectra for chiral H-aggregates with $d = 12$ Å and $N = 30$, calculated fully numerically using the one- and two-particle basis set (solid curves) and perturbatively using eq 17 (dotted curves). When the sign of J_ϕ is made negative, as in J-aggregates, the spectra take the form shown in the inset. In all cases, $\omega_0 = 1400$ cm^{-1}, $\lambda^2 = 1.1$, and $\omega_{0-0} + D_{\mathrm{agg}} = 20\,800$ cm^{-1}.

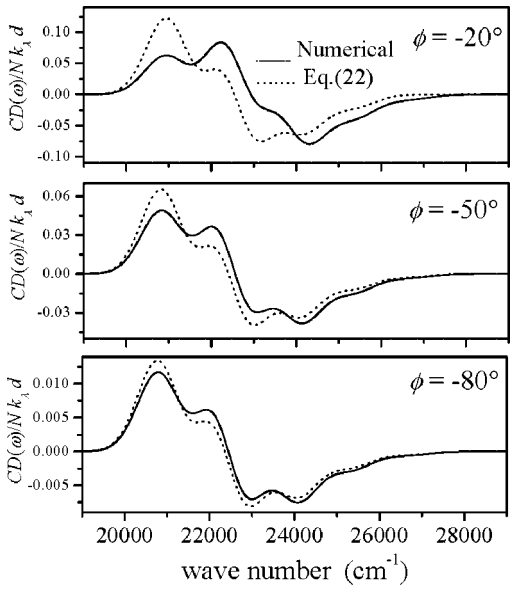

Figure 9. CD spectra for chiral aggregates with $d = 12$ Å and $N = 30$ calculated fully numerically, using the one- and two-particle basis set (solid curves), and perturbatively, using eq 22 (dotted curves). Numerical calculations employ open boundary conditions.

$\Gamma(\omega - \omega_{0-0} - D - \tilde{v}\omega_0 - f^2_{\tilde{0},\tilde{v}} J_k)$ in the small deviations, $f^2_{\tilde{v}_t,0}(J_k - J_\phi)/\sigma$ within each vibronic band. When we further insert into eq 7b the rotational line strengths from eq 10b using the first-order wave functions in eq 16, we can perform the sum over k, obtaining

$$\mathrm{CD}(\omega)/N = 4k_\lambda d \left\{ \sum_{s>0} J_{m,m+s}\, s \sin(\phi s) \right\} \times$$

$$\sum_{\tilde{v}_t} f^2_{0\tilde{v}_t} \left[f^2_{0\tilde{v}_t} \frac{\omega - \omega_{0-0} - D_{\mathrm{agg}} - \tilde{v}_t\omega_0 - f^2_{0\tilde{v}_t} J_\phi}{\sigma^2} - \mathrm{e}^{-\lambda^2} \frac{G(\tilde{v}_t;\lambda^2)}{\omega_0} \right] \times$$

$$\Gamma(\omega - \omega_{0-0} - D_{\mathrm{agg}} - \tilde{v}_t\omega_0 - f^2_{0\tilde{v}_t} J_\phi). \quad (22)$$

The spectrum takes the form of a vibronic progression of bisignate "couplets", represented by the first term in the second summand, in addition to a progression of (monosignate) Gaussians, represented by the second term, originating entirely from interband coupling. The presence of the latter means that the CD spectrum cannot be written as the derivative of the absorption spectrum, as is possible when vibronic coupling is omitted[29] or for the nearly free excitons that emerge in the strong coupling regime. However, as in the strong coupling regime, the CD signal in eq 22 remains directly proportional to the $s\sin(\phi s)$-modulated interaction sum, and therefore retains its high sensitivity to long-range interactions.

Figure 9 demonstrates the accuracy of the perturbative result in eq 22 for the loosely packed ($d = 12$ Å) helical aggregates containing $N = 30$ chromophores. The agreement with the numerical calculations involving one- and two-particle states is quite good for $|\phi|$ greater than approximately 50°.

VI. Comparison to Experiment

In this section we compare our spectra calculated using the full one- and two-particle basis set with the measured spectra of ref 13 for lutein and lutein diacetate aggregates in an acetone /water mixture. Molecular parameters are taken from the analysis of section II; i.e., the vibrational frequency is set to $\omega_0 = 1400$ cm^{-1} and the HR factor to $\lambda^2 = 1.1$. In addition, we maintained the same line width ($\sigma = 0.52\omega_0$) as that used in fitting the

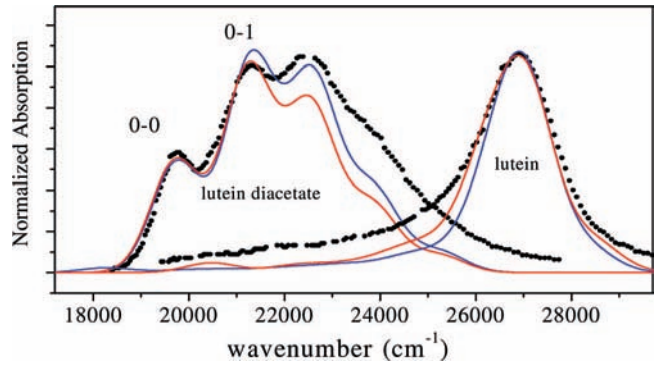

Figure 10. Numerically calculated absorption spectra for lutein and lutein diacetate aggregates using one- and two-particle states shown alongside the experimental spectra from ref 13 (black). The blue (red) curves correspond to $|\phi| = 10°$ (20°). For lutein spectra $d = 3.5$ Å, while for the lutein diacetate spectra $d = 12$ Å. For the tightly packed lutein aggregates, the value of D_{agg} was set to $D_{\mathrm{sol}} - 1700$ cm^{-1} ($D_{\mathrm{sol}} + 200$ cm^{-1}) for $|\phi| = 10°$ (20°). For lutein diacetate aggregates, D_{agg} was set to $D_{\mathrm{sol}} - 1200$ cm^{-1} for both angles.

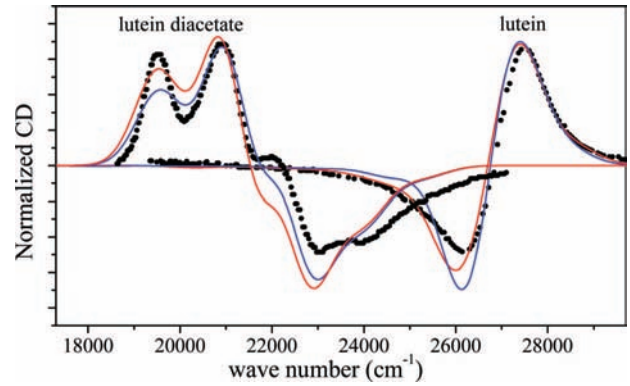

Figure 11. Numerically calculated CD spectra for lutein and lutein diacetate aggregates using one- and two-particle states shown alongside the experimental spectra from ref 13 (black). The blue (red) curves correspond to $\phi = 10°$ (20°) for lutein and $\phi = -10°$ (−20°) for lutein diacetate. For the lutein spectra $d = 3.5$ Å, while for the lutein diacetate spectra $d = 12$ Å. For the tightly packed lutein aggregates, the value of D_{agg} was set to $D_{\mathrm{sol}} - 1700$ cm^{-1} ($D_{\mathrm{sol}} + 200$ cm^{-1}) for $\phi = 10°$ (20°). For lutein diacetate aggregates, D_{agg} was set to $D_{\mathrm{sol}} - 1200$ cm^{-1} for both angles.

molecular spectrum in Figure 1. Excitonic couplings within an aggregate were evaluated as described in section III, and the spectra were evaluated numerically as described in section IV. The only adjustable parameter (aside from the obvious d and ϕ) was the difference in the aggregate and solvent shifts, $D_{\mathrm{agg}} - D_{\mathrm{sol}}$, which was chosen to fine-tune the peak alignment between theoretical and experimental spectra.

For lutein aggregates we assume tight packing, believed to be a result of hydrogen-bonding between the hydroxyl groups on both ends of the molecule.[12,13] Hence, to describe lutein aggregates, we used the value $d = 3.5$ Å typical of π-stacking. Figure 10 shows theoretical spectra for overlay angles of 10° and 20° calculated numerically (see section IV) alongside the experimental spectra from ref 13. The value $\phi = 20°$ was suggested in ref 12, based on steric effects involving the bulkier phenyl end groups. Figure 11 shows the corresponding CD spectra for both angles.

The theoretical spectra in Figure 10 accurately capture the large 6100 cm^{-1} aggregation-induced blue shift of the main absorption peak (H-band) measured with respect to the 0−0 peak in the lutein/acetone molecular spectrum (20 800 cm^{-1}).

In agreement with experiment, the calculated spectra lack vibronic structure, as strong exciton coupling induces rapid excitation transfer on a time scale much faster than a vibrational period. The spectral shift of the dominant H-band is actually the sum of a dominant excitonic blue-shift plus a smaller red-shift due to the difference $D_{agg} - D_{sol}$. For $\phi = 10°$ the excitonic blue-shift is 7780 cm^{-1}, which agrees well with the free exciton value, $J_\phi + \lambda^2\omega_0$ from eq 11. To obtain the experimental blue-shift, the value of $D_{agg} - D_{sol}$ is therefore adjusted to be -1700 cm^{-1}. For $\phi = 20°$ the excitonic shift is 5900 cm^{-1} requiring $D_{agg} - D_{sol}$ to be only $+200$ cm^{-1}. We should expect that $D_{agg} < D_{sol}$, implying that the red-shifting dispersion forces are greater when lutein is surrounded by lutein molecules, as in an aggregate, compared to lutein surrounded by less polarizable solvent molecules, as in solution. This was also suggested to be the case in ref 12.

The theoretical CD spectra for the tightly bound lutein aggregates also agree well with experiment (see Figure 11). Both theory and experiment display the classic excitonic bisignate line shape. The magnitude of the CD A value, $|A_{CD}|$, is roughly half the free exciton value in eq 14, since significant rotational oscillator strength resides in the red tail.

We next attempted to simulate the spectra for lutein diacetate aggregates shown in Figures 1 and 2 by retaining $d = 3.5$ Å and varying the overlay angle ϕ. Although increasing ϕ decreases the exciton bandwidth, the resulting absorption and CD spectral shapes were in poor agreement with experiment. We therefore increased the value of d, repeating the overlay angle analysis. Our best agreement with experiment was obtained using $d = 12$ Å, consistent with the description of such aggregates as loosely packed. Figures 10 and 11 shows the theoretical absorption and CD spectra, respectively, for overlay angles of $-10°$ and $-20°$. (The absorption spectra are invariant to the sign of ϕ). The theoretical curves do an excellent job in reproducing the experimental absorption line shape, including the line strength ratio, R_{abs}, and the peak separation, Δ_{10}. For the latter, the theoretical value of 1520 cm^{-1} compares favorably to the measured value of 1550 cm^{-1} (see Figure 6). Similarly good agreement is found for the CD spectra in Figure 11. All of the spectral positions are reproduced well by theory, although the relative intensities calculated theoretically are slightly exaggerated in the spectral window between 21 000 and 23 000 cm^{-1}.

Finally, comparing Figures 1 and 10, the aggregation-induced spectral shift for the lutein diacetate assemblies is approximately -1000 cm^{-1}. In our calculated spectra the red-shift is obtained by setting $D_{agg} - D_{sol}$ to ~ -1200 cm^{-1}, as the excitonic blue-shift for the weakly coupled H-aggregate is quite weak ($\sim$200 cm^{-1}).

VII. Lutein Diacetate Assemblies

Although the spectra of lutein diacetate aggregates are accurately reproduced using the one-dimensional helices in Figure 3, the required nearest-neighbor separation of 12 Å is too large for effective van der Waals binding. In reality, the arrangement of molecules in lutein diacetate assemblies may be similar to what is found in nematic liquid crystals, which has been suggested in several works.[5,12,13] Such assemblies consist of layers of commonly oriented carotenoid molecules with their (long) molecular axes lying within the layer plane and pointing along the nematic director. The latter rotates by ϕ degrees between consecutive layers, as depicted in Figure 12b,c. Such an assembly can be mapped onto the simpler helix in Figure 3, if one replaces each chromophore in the latter by an entire layer. In what follows we will show that, for certain intralayer packing dimensions, the absorption and CD spectra of the three-layer helices do not differ significantly from the spectra of the "1d" helices in Figure 3.

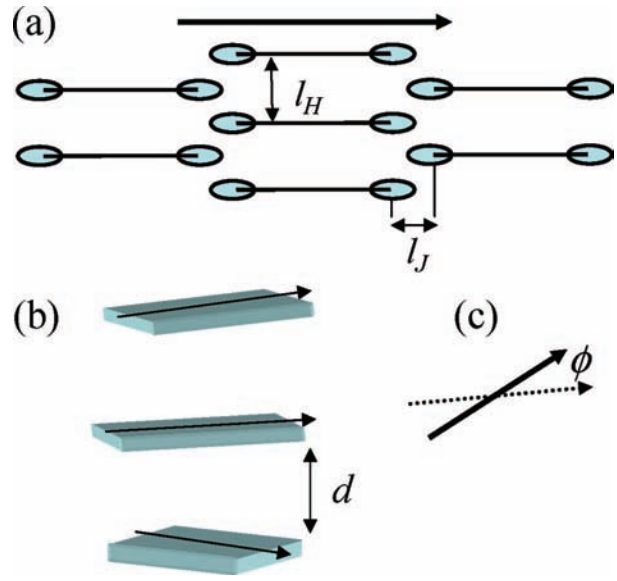

Figure 12. (a) Intralayer packing geometry of lutein diacetate assemblies viewed along the helix axis. Molecules are oriented cofacially so that the molecular plane containing the polyene core (solid lines) is normal to the layer plane. (b) Three-layer aggregate viewed from the side. The helical axis passes through the central molecule in each layer. The arrows define the directors, which are aligned according to a right-handed helix with overlay angle, ϕ, as depicted in (c).

The intralayer packing arrangement shown in Figure 12a closely resembles the model proposed for lutein dipalmitate by Bikadi et al.,[15] where the side-by-side and interlayer distances were taken to be $l_H \approx 10$ Å and $d \approx 15$ Å, respectively. Nearest neighbors are "head-to-tail" due to the association of the hydrophilic head-groups. The corresponding excitonic couplings are negative as for J-aggregates and are dependent on the distance l_J in Figure 12a. However, our calculations show that the *strongest* interactions are between the side-by-side oriented molecules. These interactions are positive (H-type) and regulated by the distance l_H. Hence, there are significant cancellations in the energy of the optically allowed ($k = 0$) intralayer exciton, causing the exciton to reside near the middle of the band and not at the band-edges as in purely J (bottom band-edge)- or H (top band-edge)-aggregates. Moreover, when the intralayer cancellations are most effective, one might expect the absorption and CD spectral line shapes in a helical stack of such layers to be dominated by the relatively weak (and positive) *inter*layer interactions that define H-aggregates. This, in effect, establishes the strong similarities between the optical responses of the two aggregates in Figures 3 and 12b.

To test our hypothesis we conducted simulations on three-layer assemblies with each layer containing the seven molecules shown in Figure 12a. We set $l_H = 10$ Å in agreement with ref 15 and varied l_J from 0 to 12 Å. In order to compare to previous calculations on the 1d helices of Figure 3, we maintained $d = 12$ Å and $\phi = -10°$. In evaluating the absorption and CD spectra, we utilized the fully numerical approach outlined in section IV with a basis set including all one- and two-particle states. The spectra for the three-layer helices are plotted in Figure 13, alongside spectra corresponding to the associated 1d helix

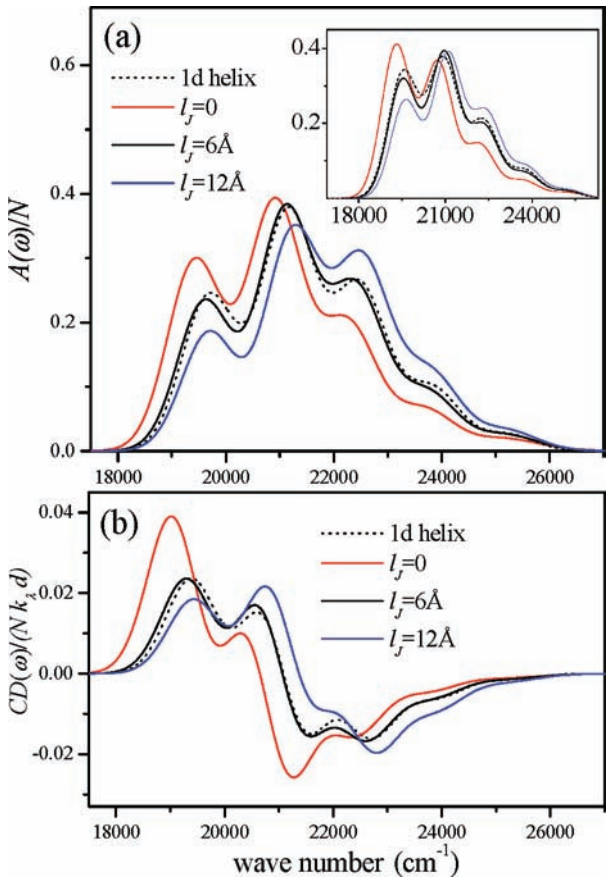

Figure 13. (a) Calculated absorption and (b) CD spectra for three-layer helical aggregates shown in Figure 13 with $l_H = 10$ Å, $d = 12$ Å, $\phi = -10°$, and various values of l_J. Also shown are the absorption and CD spectra for the corresponding 1d helix obtained by retaining only the central molecule within each layer (dotted curve). In all spectra, $D_{agg} - D_{sol} = -1200$ cm^{-1} and $\lambda^2 = 1.1$. Insert in (a) shows absorption spectra for a single seven-molecule layer for the three values of l_J alongside the single-molecule spectrum (black dashed). The single-molecule spectrum is shifted by -1200 cm^{-1} for easier comparison with the aggregate spectra.

obtained by retaining only the central molecule in each layer. It is quite striking that, despite all of the additional intra- and intermolecular interactions, the absorption and CD spectra for the three-layer helices are quite similar to the spectra for the 1d helix, with the two practically superimposable for $l_J = 6$ Å, which is approximately the width of the end-groups that cap the polyene cores.

The mechanism behind the similar spectral responses between layered and 1d helices can be traced to the optical behavior of individual layers. Absorption spectra for single layers with the three l_J values are shown in the inset of Figure 13, alongside the calculated single-molecule (monomer) spectrum from Figure 1, shifted artificially (by -1200 cm^{-1}) for easier comparison with the layer spectra. The inset shows that the single-layer spectrum for $l_J = 6$ Å closely resembles the monomer spectrum. When l_J is increased to 12 Å, the head-to-tail interactions in Figure 12a diminish, and the spectrum is characteristic of a weakly coupled *H*-aggregate where the 0−0 to 0−1 intensity ratio is significantly reduced compared with the monomer. Conversely, when l_J is reduced to zero, the head-to-tail interactions prevail, and the spectrum is characteristic of a weakly coupled *J*-aggregate with a more pronounced 0−0 peak.

The behavior described above can be better understood by appealing to first-order perturbation theory introduced in section V. When the exciton coupling within layers is weak, deviations of the vibronic peak *intensities* from the single-molecule values are governed by $J^{layer}_{k=0}/\omega_0$, where $J^{layer}_{k=0} \equiv \sum_{\mathbf{s}} J_{\mathbf{n},\mathbf{n}+\mathbf{s}}$ is the resonance energy of the optically allowed $k = 0$ "layer" exciton.[49] The sum in $J^{layer}_{k=0}$ is over all intermolecular separations, $\mathbf{s}$, within the layer. For the layer geometry in Figure 12a, the sum contains four nearest-neighbor *J*-type interactions and two next-nearest-neighbor *H*-type interactions. For $l_J = 6$ Å, we calculate $-0.158\omega_0$ for each *J*-interaction and $+0.332\omega_0$ for each *H*-interaction. Hence, the sum in $J^{layer}_{k=0}$ is largely canceled, rendering the first-order correction to the spectral intensities practically zero and resulting in a single-layer spectrum resembling that of a single molecule. When l_J is reduced to zero, the head-to-tail interactions are increased by almost a factor of 2 (the *H*-interactions are unaffected). In this case $J^{layer}_{k=0}$ is substantial and negative, and the spectrum in the inset of Figure 13a corresponds to a *J*-aggregate with an enhanced 0−0 peak (see also Figure 8). Increasing l_J to 12 Å reduces the head-to-tail interactions by about a factor of 2, allowing the *H*-interactions to prevail and yielding spectra consistent with weakly coupled *H*-aggregates.

We have also evaluated $J^{layer}_{k=0}$ for much larger layers containing several thousand chromophores. The point at which the intermolecular interactions cancel out—the null point—shifts to slightly larger l_J values compared with the seven-molecule layer in Figure 12a. At convergence (~1000 molecules) the null point is achieved when l_J is approximately 7.4 Å, an increase of only 1.4 Å from the seven-molecule layer in Figure 12a but still within the physically reasonable range for the loosely packed lutein diacetate layers.

We now consider the helical stack of layers shown in Figure 12b. Near the null point, the sum over all interactions between a central molecule in one layer and all molecules in a neighboring layer is dominated by J_{cm}, where J_{cm} is the interaction between just the two central molecules. For example, for large layers containing ~2000 molecules each, the aforementioned interaction sum is about $0.8J_{cm}$ when $l_J = 7.4$ Å. Therefore, very similar spectral line shapes for the layered aggregates in Figure 12a and the 1d helices in Figure 3 are expected when

$$|J^{layer}_{k=0}| \ll J_{\phi} \tag{23}$$

where J_ϕ, defined in eq 12, corresponds to the 1d helix formed from the central molecules in each layer. Taking $d = 12$ Å and $\phi = -10°$, we obtain $J_\phi \approx 0.5\omega_0$, which can easily overtake $|J^{layer}_{k=0}|$ for reasonable values of l_J within several angstroms of the null point. Furthermore, because the measured spectral red-shift for lutein diacetate assemblies is a respectable 1000 cm^{-1}, it is likely that head-to-tail intralayer interactions also contribute to the spectral shift (i.e., $J^{layer}_{k=0} < 0$). The effect is observed in Figure 13, where decreasing l_J from 12 Å to 0 (coincident with increasingly negative head-to-tail interactions) leads to a spectral red-shift of approximately 250 cm^{-1}. A more definitive determination of the relative contributions from resonant and nonresonant interactions will require more detailed information about the intralayer packing.

(49) The resonance energy for the optically allowed exciton is strictly valid for infinite layers or finite layers with periodic boundary conditions. For finite aggregates with open boundary conditions, it remains approximately correct.

VIII. Discussion and Conclusion

It is quite remarkable that the simple helices of Figure 3 can account for the very different spectral characteristics of lutein and lutein diacetate assemblies. Our results show the former to be tightly packed *H*-aggregates with nearest-neighbor distances and overlay angles in the ranges $d \approx 3-4$ Å and $\phi \approx 10-20°$, respectively. Our d value is smaller than that predicted by Zsila et al.[13] (~5 Å), but those authors utilized point dipole−dipole coupling in their analysis, which overestimates the actual coupling at distances d smaller than the molecular (conjugation) length. As suggested in ref 13, the tight binding is likely aided by hydrogen-bonding involving the two terminal hydroxyl hydrogens in lutein. When these are replaced by $-COCH_3$ groups, the capacity for hydrogen-bonding is lost, and the resulting lutein diacetate aggregates become loosely packed.[12,13]

The helical array of chromophores in Figure 3 can also describe the spectral line shapes of lutein diacetate assemblies that (unlike lutein assemblies) retain vibronic structure. In particular, the model successfully accounts for the aggregation-induced reduction of the 0−0 peak intensity relative to the 0−1 peak intensity in the absorption spectrum—shown here to be a clear signature of *H*-aggregation—as well as the enhanced spectral separation between the 0−0 and 0−1 spectral positions. Such effects have also been observed in P3HT thin films[24,25] as well as perylene-based thin films[50] and nanoassemblies.[51] However, despite the satisfactory agreement between the measured and calculated spectra, the nearest-neighbor distance ($d \approx 12$ Å) required for optimal agreement with experiment is too large for van der Waals binding. Moreover, at such distances it is difficult to rationalize the measured 1000 cm^{-1} red-shift of the absorption spectrum upon aggregation entirely in terms of nonresonant dispersion interactions. Hence, we turned to the nematic liquid crystal model of Bikadi et al.[13,15] Surprisingly, the helical layer arrangement of Figure 12b with $l_H = 10$ Å and l_J in the range 4−7 Å gives essentially the same absorption and CD line shapes as the associated 1d helix formed from the central molecule in each layer. The line shapes are dominated by *inter*layer interactions and reflect weak *H*-aggregation despite the existence of significant head-to-tail (*J*-type) interactions which can actually exceed (in magnitude) the interlayer *H*-type interactions.

Analysis of the individual layers based on the geometry of Figure 12a showed the existence of a "null" point—a particular value of l_J (for a given l_H) at which the sum over the excitonic interactions ($J_{k=0}^{layer}$) is zero due to an effective cancelation of all intralayer *J*- and *H*-type interactions. An immediate implication is that the spectral shift of the optically allowed exciton ($J_{k=0}^{layer}$) is zero; in other words, the layer is exactly intermediate between a *J*- and *H*-aggregate. (This does not imply that the exciton bandwidth also vanishes.) In the limit of large layers, in which convergence is assured, the null point occurs at $l_J \approx 7.4$ Å when $l_H = 10$ Å, a physically accessible point for the loosely packed lutein diacetate chromophores. The most surprising property of aggregates near the null point is their optical response: near the null point the absorption and CD line shapes of an entire layer closely resemble their single-molecule counterparts, and the optical response of a helical stack of layers resembles that displayed by a 1d helix created by retaining only the central molecule in each layer. The existence of the null point also allows considerable freedom for molecular sliding along the nematic direction, as would occur in actual liquid crystals, in a manner that would not dramatically increase the spectral line widths. A principle similar to the null point is also at work in polymer aggregates, where the excitonic interaction between two (parallel) polymers has been shown to vanish as the conjugation length increases to values much greater than the interpolymer separation.[52−55] However, in this example the entire bandwidth vanishes as well.

Although our calculations show the measured 1000 cm^{-1} red-shift in lutein diacetate assemblies to be dominated by nonresonant intralayer dispersion forces, we cannot discount an additional component due to the intralayer excitonic (head-to-tail) interactions without more detailed knowledge of the intralayer packing. It is probable that l_J is smaller than the null value of 7.4 Å, allowing the *J*-interactions within each layer to prevail ($J_{k=0}^{layer} < 0$) and resulting in an excitonic component to the overall spectral red-shift. In such hybrid aggregates the optical spectra are *H*-like with respect to shape (assuming condition (23) continues to hold) and *J*-like with respect to the aggregation-induced spectral shift.

Our conclusions regarding the liquid crystal model are strictly valid under the condition of weak intralayer excitonic coupling. For the layers in Figure 12a, we find that perturbation theory remains accurate when $e^{-\lambda^2} W_{layer}/\omega_0 \lesssim 1/2$, i.e., when the vibronic bands are well separated. Here, W_{layer} is the (free) exciton bandwidth for a given layer. The unusual single-molecule response near the null point exists despite relatively large values of W_{layer} because the first-order changes to the spectral line shapes depend *not* on W^{layer}/ω_0 but on $J_{k=0}^{layer}/\omega_0$. At the null point, the totally destructive interference among excitonic interactions within $J_{k=0}^{layer}$ critically depends on the inclusion of all extended interactions. For example, making the nearest-neighbor approximation (NNA) on the layer aggregates in Figure 12a results in $J_{k=0}^{layer} = -W^{layer}/2$. There is no null point, and the first-order spectral changes are now proportional to W^{layer}/ω_0. In our previous studies of one-dimensional π-stacks of P3HT,[24,38,39] we invoked the NNA, thereby validating first-order corrections to the line intensities in terms of W/ω_0. However, in 1d the NNA is most accurate, as the null point is physically realizable in two or three dimensions.

When the bandwidth increases beyond the perturbative regime, the spectral response at the null point is no longer expected to resemble the single-molecule response. For example, if l_H is reduced from 10 Å to 6 Å, we find that the null point occurs for l_J closer to 3 Å and W_{layer} increases beyond the weak coupling regime. In this case the absorption spectrum has a much greater red-shift due to the stronger participation of two-particle states. We are currently investigating such strong coupling effects further.

Our results for the helices of Figure 3 show that the sensitivity of CD spectroscopy to long-range interactions is maintained in the presence of exciton−vibrational coupling, with the modulated interaction sum, $\sum_{s>0} J_{n,n+s}\, s \sin(\phi s)$, appearing as a prefactor for CD(ω) in the strong and weak excitonic coupling regimes (see eqs 14 and 22). In dimeric systems ($N = 2$) this

(50) Heinemeyer, U.; Scholz, R.; Gisslen, L.; Alonso, M. I.; Osso, J. O.; Garriga, M.; Hinderhofer, A.; Kytka, M.; Kowarik, S.; Gerlach, A.; Schreiber, F. *Phys. Rev. B* **2008**, *78*, 085210.
(51) Shaller, A. D.; Wang, W.; Gan, H. Y.; Li, A. D. Q. *Angew. Chem., Int. Ed.* **2008**, *47*, 7705.
(52) McIntire, M. J.; Manas, E. S.; Spano, F. C. *J. Chem. Phys.* **1997**, *107*, 8152.
(53) Manas, E. S.; Spano, F. C. *J. Chem. Phys.* **1998**, *109*, 8087.
(54) Cornil, J.; dos Santos, D. A.; Crispin, X.; Silbey, R.; Bredas, J. L. *J. Am. Chem. Soc.* **1998**, *120*, 1289.
(55) Barford, W. *J. Chem. Phys.* **2007**, *126*, 134905.

sensitivity has been well documented, with CD signals detectable for two chromophores separated by as much as 40−60 Å.[46−48] For long chiral stacks the long-range sensitivity has been demonstrated theoretically in ref 30, where it was shown that truncating the excitonic interactions after the seventh nearest neighbor leads to a 30% increase in the CD signal with practically no change in the (unpolarized) absorption spectrum. In addition, in their analysis of helical cylindrical aggregates, Didraga et al.[28,29] have shown that the CD spectrum remains size-dependent at a point where the absorption spectrum has fully converged. We believe that CD spectroscopy in helical assemblies holds great promise for unraveling the fundamental nature of intermolecular interactions, including the elusive aspects of dielectric screening.

Finally, we have shown that a basis set consisting of vibronic and vibronic/vibrational excitons is quite effective for treating exciton−vibrational coupling in organic assemblies. Inclusion of the far more numerous vibronic/vibrational states ensures a quantitative description of the absorption and CD line shapes with increasing exciton bandwidth (see Figure 6). Two-particle states play a much larger role in emission,[33−36] even in the weak excitonic coupling regime.[38] Such states also determine the extent (or radius) of the phonon cloud of the emitting exciton, or neutral excitonic polaron,[30] and should play a major role in transport dynamics.

Acknowledgment. F.C.S. is supported by the NSF, grant DMR No. 0606028.

Supporting Information Available: Further details pertaining to the calculation of the excitonic coupling J_{mn} between molecules m and n. This information is available free of charge via the Internet at http://pubs.acs.org.

JA806853V